Quality Engineering
Publication details, including instructions for authors and subscription information:
http://www.tandfonline.com/loi/lqen20

Process Optimization for Multiple Responses Utilizing the Pareto Front Approach

Jessica L. Chapman [a] , Lu Lu [b] & Christine M. Anderson-Cook [c]
[a] Department of Mathematics, Computer Science, and Statistics , St. Lawrence University , Canton , New York
[b] Department of Mathematics and Statistics , University of South Florida , Tampa , Florida
[c] Statistical Science Group , Los Alamos National Laboratory , Los Alamos , New Mexico
Published online: 27 May 2014.

To cite this article: Jessica L. Chapman , Lu Lu & Christine M. Anderson-Cook (2014) Process Optimization for Multiple Responses Utilizing the Pareto Front Approach, Quality Engineering, 26:3, 253-268, DOI: 10.1080/08982112.2013.852681

To link to this article: http://dx.doi.org/10.1080/08982112.2013.852681

Quality Engineering, 26:253–268, 2014

ISSN: 0898-2112 print/1532-4222 online
DOI: 10.1080/08982112.2013.852681

Taylor & Francis
Taylor & Francis Group

Process Optimization for Multiple Responses Utilizing the Pareto Front Approach

Jessica L. Chapman[1], Lu Lu[2], Christine M. Anderson-Cook[3]

[1]Department of Mathematics, Computer Science, and Statistics, St. Lawrence University, Canton, New York
[2]Department of Mathematics and Statistics, University of South Florida, Tampa, Florida
[3]Statistical Science Group, Los Alamos National Laboratory, Los Alamos, New Mexico

ABSTRACT In many optimization situations, there are several responses associated with a product or process that need to be jointly considered. In this article we present Pareto front multiple objective optimization as an option to complement other statistical and mathematical methods in the response surface methodology toolkit. We demonstrate the Pareto front approach for multiple response process optimization based on evaluating a fine grid of input variable combinations within the range of operating conditions, as well as the use of a set of graphical tools to aid in decision making, with an example process involving two inputs and three responses of interest. We also discuss a simple way to examine the impact that variability in the responses can have on the solution by considering the estimated mean and worst-case response values. R code for implementing the methods discussed in this article is available upon request (jchapman@stlawu.edu).

KEYWORDS graphical summary, multiple response optimization, response surface, trade-offs

INTRODUCTION

In many optimization situations, there are several responses associated with a product or process that need to be jointly considered for improved decision making. For example, Myers et al. (2009, p. 253) described a chemical process involving two input variables ($\xi_1 =$ time and $\xi_2 =$ temperature) and three responses of interest ($y_1 =$ yield, $y_2 =$ viscosity, $y_3 =$ number-average molecular weight). In this example, it is desired to identify the set of operating conditions that jointly optimizes the three responses. The optimization problem can be formulated with the objective of simultaneously maximizing yield while minimizing both molecular weight and the distance between the viscosity and a target value of 65, the midpoint of the desired range (62 to 68) specified in Myers et al. (2009). It is believed that the optimal operating conditions occur when the time of the process is between 77 and 93 min and when the temperature is between 167 and 183°F. It is also believed that either a second-order or simpler model is appropriate for all of the responses in this region. To investigate this region of operating

Address correspondence to Jessica L. Chapman, Department of Mathematics, Computer Science, and Statistics, St. Lawrence University, 23 Romoda Dr., Canton, NY 13617. E-mail: jchapman@stlawu.edu

Color versions of one or more of the figures in the article can be found online at www.tandfonline.com/lqen.

TABLE 1 Central Composite Design with Three Responses from Myers et al. (2009, p. 253)

Natural variables		Coded variables		Responses		
ξ_1 (time)	ξ_2 (temperature)	x_1	x_2	y_1 (yield)	y_2 (viscosity)	y_3 (molecular weight)
80	170	−1	−1	76.5	62	2,940
80	180	−1	1	77.0	60	3,470
90	170	1	−1	78.0	66	3,680
90	180	1	1	79.5	59	3,890
85	175	0	0	79.9	72	3,480
85	175	0	0	80.3	69	3,200
85	175	0	0	80.0	68	3,410
85	175	0	0	79.7	70	3,290
85	175	0	0	79.8	71	3,500
92.07	175	1.414	0	78.4	68	3,360
77.93	175	−1.414	0	75.6	71	3,020
85	182.07	0	1.414	78.5	58	3,630
85	167.93	0	−1.414	77.0	57	3,150

conditions, an experiment using a central composite design (Myers et al. 2009, p. 297) was run. The design points (on the natural and coded scales) as well as the observed responses from this experiment are displayed in Table 1.

Complete second-order models were fitted for each of the three responses independently. However, when molecular weight was used as the response variable, none of the higher order terms were significant (at any reasonable significance level), suggesting that a first-order model would suffice. The three fitted models are as follows:

$$\widehat{y_1} = 79.94 + 0.995x_1 + 0.52x_2 + 0.25x_1x_2 - 1.38x_1^2 - 1.00x_2^2$$

$$\widehat{y_2} = 70.0 - 0.16x_1 - 0.95x_2 - 1.25x_1x_2 - 0.69x_1^2 - 6.69x_2^2$$

$$\widehat{y_3} = 3386.2 + 205.1x_1 + 177.4x_2.$$

Contour plots displaying each of the estimated response surfaces are shown in Figure 1. The maximum yield, near 80, occurs for times between 85 and 89 min and temperatures between 173 and 179°F. The contour plot for molecular weight indicates that decreasing both time and temperature results in the desired lower molecular weight. The contour plots on the right side of Figure 1 display the estimated response surface for viscosity (top) and distance between the estimated viscosity and the target viscosity 65, which we would like to minimize (bottom). This target can be achieved at nearly any time in the operating range when the temperature is near either 171 or 178°F.

Simultaneously optimizing the three responses will clearly require some trade-offs to be made, particularly between yield and molecular weight as the optimal inputs for one differ considerably than those for the other. Overlaying the contour plots, as displayed in Figure 2, is an informal method by

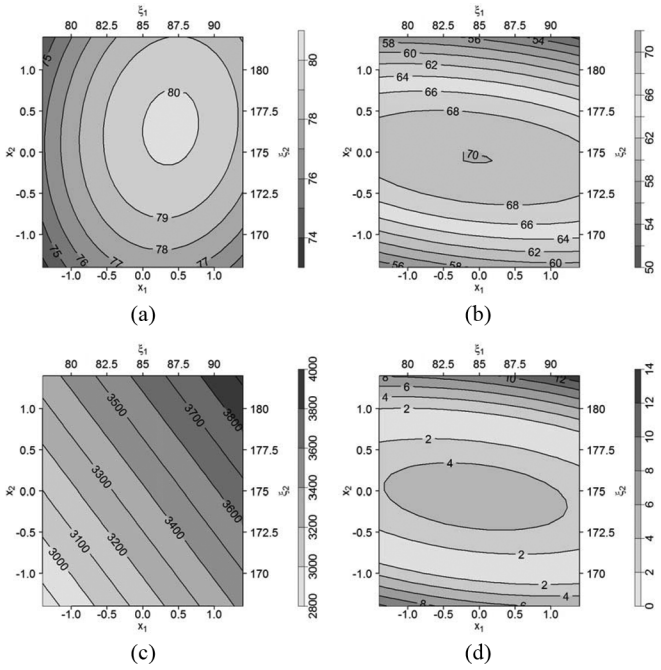

FIGURE 1 Contour plots for each of the estimated response surfaces for the three responses and the distance between the estimated viscosity and its target of 65. Lighter colors indicate better values of the criteria: (a) yield; (b) viscosity; (c) molecular weight; and (d) |Viscosity −65|.

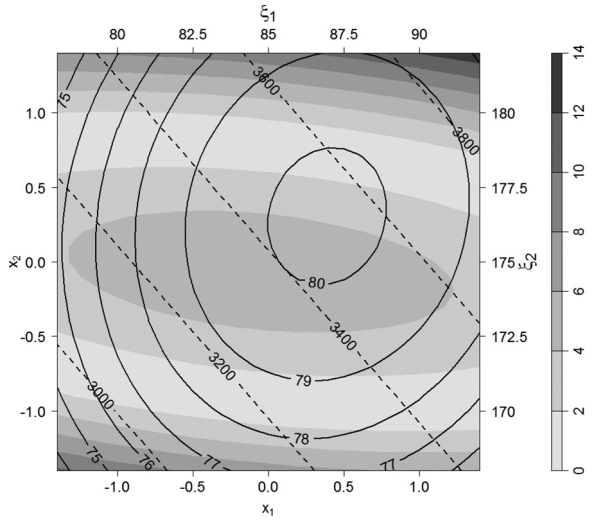

FIGURE 2 **Overlaid contours plots for the three estimated response surfaces. The grayscale contours correspond to distance between the estimated viscosity and the target viscosity of 65, with lighter colors indicating better values. The solid line contours correspond to the yield criterion. The dashed line contours correspond to the molecular weight criterion.**

which the three responses could be considered simultaneously to suggest potentially promising regions with adequate performance for all of the responses. When looking for the optimal solution, one should consider the lighter shaded regions (corresponding to near-optimal values of the viscosity criterion) with at least moderately good performance for both of the other criteria. However, it is difficult to identify a specific best solution to implement or to compare the merits of competing solutions with this approach.

In this article, we use a Pareto front approach to aid in identifying the operating conditions that simultaneously optimize the three responses by examining a fine grid of points within the region considered. In the following section we provide some background on Pareto front multiple objective optimization and use the Pareto front approach to identify a solution for the optimal operating conditions of the process based on the estimated response surfaces for the three response variables. Then we compare the Pareto front solutions to those obtained by alternative approaches presented in Myers et al. (2009, pp. 260–262). Due to the uncertainty associated with estimated response surfaces as well as the natural variability in the response of the process, a simple approach for investigating the impact of variability in predicting the responses and on the Pareto front is presented in the next section. We conclude with some final remarks and discussion of future work.

PARETO FRONT MULTIPLE OBJECTIVE OPTIMIZATION

Multiple Objective Optimization

Myers et al. (2009) described two possible ways to identify the optimal operating conditions for this chemical process approximated by the estimated response surfaces: formulating the problem as a constrained optimization problem and using desirability functions. Constrained optimization focuses on one response as the primary goal, subject to one or more constraints. In this case, where yield is considered the primary response, Myers et al. (2009) suggested formulating the problem as optimizing yield subject to constraints on viscosity and molecular weight:

$$\text{Maximize}\,\hat{y}_1\,,\,\text{subject to}\,62 \le \hat{y}_2 \le 68\,\text{and}\,\hat{y}_3 \le 3400.$$

This type of problem is encountered frequently in the field of operations research, and common solutions are found by direct search and numerical optimization methods. Carlyle et al. (2000) provided an overview of these methods useful in situations such as this. The solutions found by Myers et al. (2009) via constrained optimization are presented in Table 2.

The desirability function (DF) approach of Derringer and Suich (1980) is commonly used to simultaneously optimize multiple objectives, particularly in the area of design of experiments. In the DF approach, the different criteria are converted to a common desirability scale, typically between 0 (worst) and 1 (best), and are combined to create a single summary of the overall merit of a possible solution. Common forms of the DF are additive and multiplicative desirability. In the case of optimizing three objectives, the additive DF is expressed as

$$DF_{add}(j,w) = w_1C_1(j) + w_2C_2(j) + w_3C_3(j),$$

where $C_i(j)$ represents the scaled value for criterion i for solution j, for $i=1$, 2, 3, and w is the weight vector, with $w_i \ge 0$ representing the user-specified weight given to criterion i and $\sum_{i=1}^{3} w_i = 1$. The multiplicative DF is expressed as

$$DF_{mult}(j,w) = C_1(j)^{w_1} \cdot C_2(j)^{w_2} \cdot C_3(j)^{w_3}.$$

The additive form of the DF allows for the very good performance of one or more of the criteria to override poor performance by another criterion,

TABLE 2 Solutions Presented in Myers et al. (2009) Found via Constrained Optimization and Desirability Functions

Method		Optimal operating conditions	Estimated responses
Constrained optimization	#1	$\xi_1 = 83.5$ and $\xi_2 = 177.1$	$\hat{y}_1 = 79.6$, $\hat{y}_2 = 68.6$, $\hat{y}_3 = 3{,}399$
	#2	$\xi_1 = 86.6$ and $\xi_2 = 172.25$	$\hat{y}_1 = 79.6$, $\hat{y}_2 = 68.6$, $\hat{y}_3 = 3{,}354$
Desirability function	#1	$\xi_1 = 86.1$ and $\xi_2 = 170.3$	$\hat{y}_1 = 78.7$, $\hat{y}_2 = 65.2$, $\hat{y}_3 = 3{,}264$
	#2	$\xi_1 = 80.3$ and $\xi_2 = 179.2$	$\hat{y}_1 = 77.7$, $\hat{y}_2 = 65.0$, $\hat{y}_3 = 3{,}342$

whereas the poor performance of a single criterion is more strongly penalized with the multiplicative form. Since the weights capture user prioritization about the criteria, the choice of "best" design is strongly influenced by the w_is, the scaling schemes, and the DF forms. Making a decision without understanding the impact of these subjective choices can be risky.

Myers et al. (2009) used the multiplicative DF with the three criteria being weighted as equally important to find two solutions. To scale the yield variable, they specified a target of 80 for the maximum yield and 70 as the lowest acceptable yield. Viscosity is scaled so that the target viscosity is 65 and the minimum and maximum acceptable viscosities are 62 and 68, respectively. The final variable, molecular weight, is scaled by specifying 3,200 to 3,400 as the acceptable range (see Myers et al. 2009, p. 261). The corresponding desirability solutions suggested in Myers et al. (2009) are displayed in Table 2.

Another technique, the Pareto front approach, has been extensively used in many disciplines as a tool for optimizing multiple responses (Gronwald et al. 2008; Kasprzak and Lewis 2001; Trautmann and Mehnen 2009). Lu et al. (2011) adapted the Pareto front approach for design of experiments problems and enhanced it with graphical assessment tools to aid in the decision-making process. The method consists of two stages: (1) the objective Pareto optimization step, where poor candidates (strictly inferior to others) are removed from the set of contenders, and (2) the subjective decision analysis step, where solutions from the Pareto front are examined to investigate trade-offs between the criteria and robustness to different weightings of the criteria. The objective step of identifying the Pareto front allows the experimenter to see the full set of competing choices before considering the subjective aspects of the decision, which can be tailored to match study goals.

A solution is said to *Pareto dominate* another if it is at least as good for all criteria and strictly better for at least one. The *Pareto set* contains all solutions that are not Pareto dominated by others, and their corresponding criteria vectors form the *Pareto front* in the criteria space. Geometrically, the Pareto set consists of the points on the outer edge of all obtainable solutions closest to the ideal value for each objective (illustrated in Figure 3). In the Pareto front literature, the *utopia point* is defined as the vector that simultaneously achieves the best values for all criteria, but because of trade-offs between objectives it is generally not attainable. The Pareto set represents the collection of points from which a solution should be selected, as any dominated point has at least one better alternative on the Pareto front. Lu et al. (2011) described how to use an adapted utopia point approach to reduce a large Pareto set to a smaller, more manageable set of solutions for the decision-making step.

Solutions on the Pareto front can be evaluated on three different aspects: (1) performance for a particular set of weights which match the user's study goals, (2) robustness of the solution based on a range of weightings close to user preferences, and (3) performance as measured as a synthesized efficiency

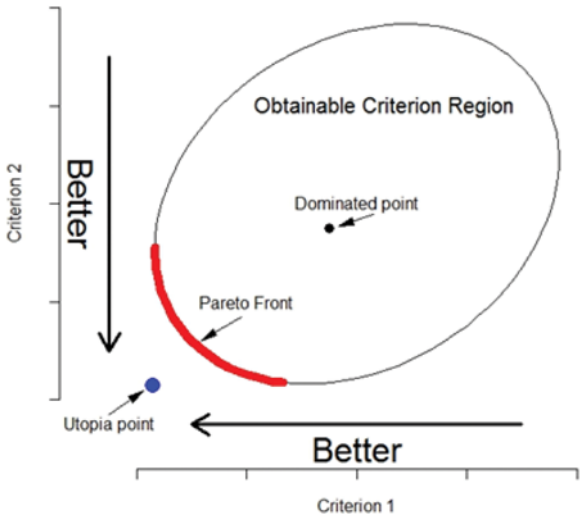

FIGURE 3 Illustration of Pareto front when two criteria are being minimized simultaneously.

relative to the best allocation possible for a particular set of weight choices (Lu and Anderson-Cook 2012). A final decision about the optimal solution should be made by the user based on the priorities of the study after considering the trade-offs between candidate solutions and the robustness of candidate solutions to different subjective choices. Compared to the standard DF method, the Pareto approach provides summaries of what range of solutions are available, more intuition about the relative performance of different solutions, and quantitative information for making a defensible choice.

Pareto Front Approach for Optimizing the Chemical Process

To create a set of solutions from which we identify the Pareto set, we first define a grid of 630 points, displayed in Figure 4, that fill in the circular region defined by the points used for the central composite design. Adjacent points in the same row or column of the grid are separated by a distance of 0.1 for the scaled variables, since this was assumed to match the finest gradation possible when setting the factor levels. The points on the grid are labeled from 1 to 630 beginning with the bottom row of points in Figure 4 and moving from the left to the right. Once the end of a row is reached, the labeling system wraps around to continue with the leftmost point of the next lowest row. The labels of the leftmost points for each row on the grid are listed along the left edge of Figure 4.

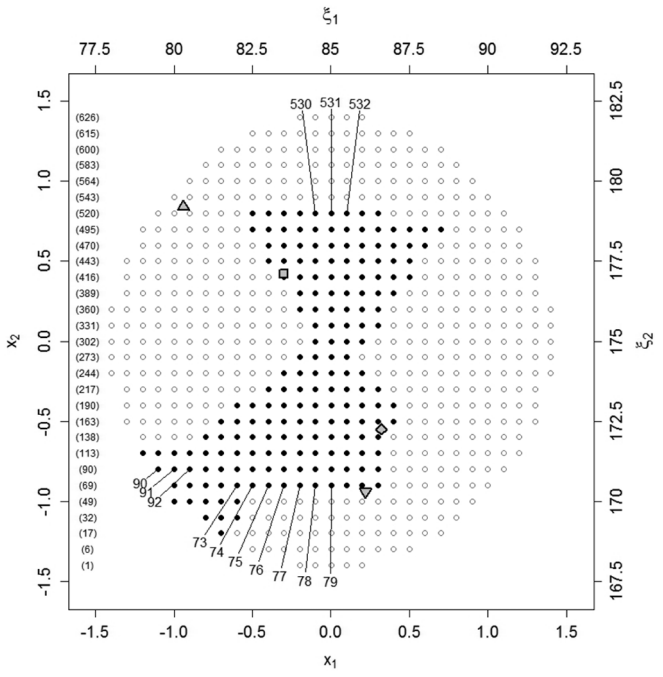

FIGURE 4 **Grid of points used to approximate response surfaces for each response and the resulting Pareto front (dark points). The solutions from Table 2 are also displayed (square = constrained optimization #1, diamond = constrained optimization #2, inverted triangle = desirability function #1, and triangle = desirability function #2). Labeled solutions are those identified as optimal for at least 1% of weights when the multiplicative DF is used (see Figure 6).**

The grid of points and the fitted models were used to approximate response surfaces for each of the three response variables. From this set of 630 possible solutions, the Pareto set was identified; the set consists of 181 solutions that are contenders for simultaneously maximizing yield, achieving a target viscosity of 65, and minimizing molecular weight. The locations of the Pareto solutions, considered on both the coded and natural variable scales, are displayed in Figure 4 with the points on the front identified by the dark closed points. Overlaid square and diamond points indicate solutions (#1 and #2, respectively) identified by Myers et al. (2009) via constrained optimization, and the solutions found using the desirability function approach are displayed with inverted triangular (#1) and triangular (#2) symbols. We notice immediately that three of the four solutions presented in Myers et al. (2009) are close to points on the Pareto front, and one of the desirability solutions (#2) lies well away from the front.

Figure 5 displays pairwise scatterplots of the estimated responses, with points on the three criteria Pareto front represented by the darker points. In each plot, dashed lines are used to identify the optimal estimation for each response, and thus the intersection of lines on the plot displays the utopia point for the two criteria. It is apparent that there is considerable trade-off between yield and molecular weight, since no points are close to the utopia point for this pairwise plot. The solutions identified from Myers et al. (2009) are close to the Pareto front except for solution desirability #2, which is clearly outperformed by many possible solutions on the Pareto front. Both DF solutions achieve the target value for viscosity with some sacrifices in the other two responses.

Identifying the Pareto front eliminates all but 181 of the locations as contenders for the best solution to simultaneously optimize the three responses. However, the user must ultimately choose a single

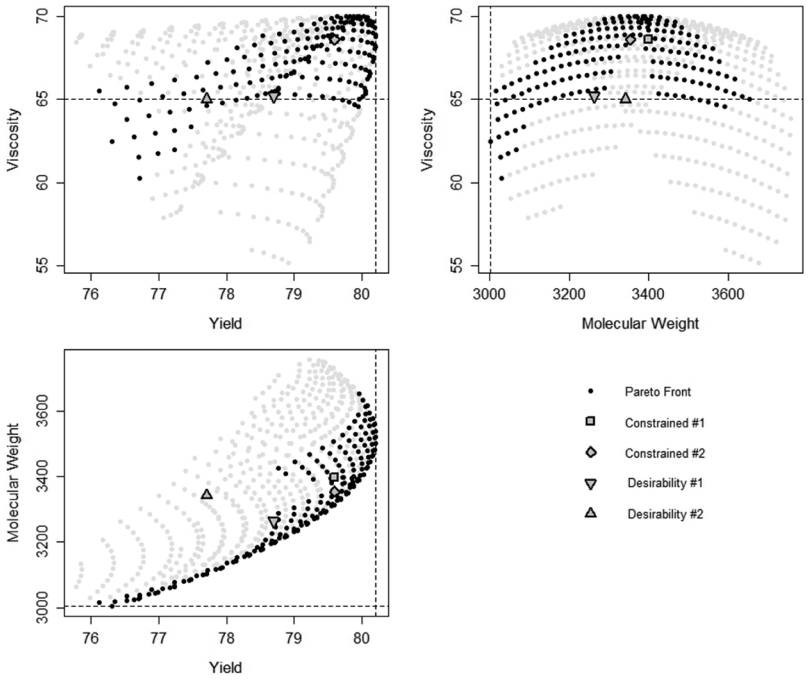

FIGURE 5 **Pairwise scatterplots of estimated responses, with points on the three-criteria Pareto front identified as the dark points.**

solution as the recommended optimal setting for the process. Next, we illustrate how to examine the performance robustness of contending solutions across different prioritizations while examining the trade-offs between solutions.

In this situation, since we may have little a priori knowledge about the relative importance of the three criteria, we explore all possible weighing schemes to see how the choice of the optimal design location varies. We scale each of the three criteria so that the best value on the front maps to 1 and the worst maps to 0. Additionally, we must choose how to combine the individual scaled criteria values into a single metric. For the remaining decision analysis, we choose the multiplicative form of the DF to be consistent with Myers et al. (2009). The choice of scaling and the form of the desirability function are subjective decisions that should match user priorities and do influence subsequent results. If the experimenter is uncertain about these choices, a sensitivity analysis is recommended. This requires little extra computational effort once the Pareto front has been identified.

Figure 6 displays the mixture plot (or simplex) of the best solutions for different weightings of the three criteria (Lu et al. 2011), using a multiplicative desirability function. The vertices and the edges correspond to optimization based on a single criterion and two of the three criteria, respectively. More detailed description of the mixture plot is available in Cornell (2002, p. 24). Of the 181 solutions on the Pareto front, 13 are identified as being optimal for a relatively large percentage of the possible weightings considered (at least 1% of the total simplex area). Additionally, solution 484, which is optimal when yield is weighted around 80% and

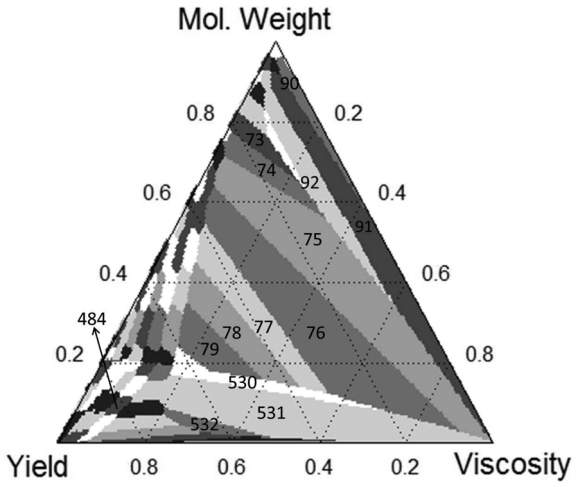

FIGURE 6 **Mixture plot based on using the multiplicative desirability function. The 13 solutions that are optimal for at least 1% of weighting space are labeled in their corresponding regions. Allocation 484 is also highlighted as a promising solution when yield is weighted around 80% and the remaining two criteria are weighted equally.**

TABLE 3 The 13 Solutions Identified as Optimal for more than 1% of the Weights Considered in the Mixture Plot (Figure 6) Based on Using Multiplicative DF. Allocation 484 is also Included as a Promising Solution when Yield is Weighted Around 80% and the Remaining Two Criteria are Weighted Equally

		Coded variables		Natural variables		Estimated responses		
Solution #	% Area in mixture (Figure 6)	x_1	x_2	ξ_1	ξ_2	$\hat{y}_1$	$\hat{y}_2$	$\hat{y}_3$
73	1.44	−0.6	−0.9	82	170.5	77.70	64.61	3,103.48
74	2.38	−0.5	−0.9	82.5	170.5	77.93	64.78	3,123.99
75	16.54	−0.4	−0.9	83	170.5	78.14	64.94	3,144.47
76	16.68	−0.3	−0.9	83.5	170.5	78.31	65.08	3,164.99
77	5.07	−0.2	−0.9	84	170.5	78.46	65.21	3,185.50
78	4.43	−0.1	−0.9	84.5	170.5	78.57	65.33	3,206.03
79	3.04	0	−0.9	85	170.5	78.66	65.44	3,226.54
90	1.26	−1.1	−0.8	79.5	171	76.35	64.72	3,018.62
91	8.16	−1	−0.8	80	171	76.72	64.95	3,039.13
92	3.70	−0.9	−0.8	80.5	171	77.05	65.16	3,059.69
484	0.29	0.2	0.6	86	178	80.06	66.81	3,533.60
530	1.87	−0.1	0.8	84.5	179	79.58	65.07	3,507.61
531	11.82	0	0.8	85	179	79.71	64.96	3,528.05
532	1.10	0.1	0.8	85.5	179	79.82	64.84	3,548.63

the other two criteria are weighted equally, is also identified. Table 3 reports the actual mixture area for each of these highlighted solutions; the 13 more robust (larger area) solutions are labeled in Figure 4.

Solutions 75 and 76 are each the optimal solution for about 17% of the weights considered (Table 3) and account for the largest areas in Figure 6. The weightings for which solution 75 is optimal range from all weight to very little weight on viscosity with more weight on molecular weight than yield. Solution 76 generally gives more weight to yield compared to solution 75 and balances the three criteria more evenly, including the case where the three criteria are equally weighted. Solution 531 is optimal for about 12% of the weights considered (Table 3), specifically those that put more emphasis on yield and/or viscosity but little emphasis on the molecular weight. Solution 91 is optimal for about 8% of the weights considered (Table 3), specifically those that put little emphasis on yield. Finally, the corner corresponding to the best yield consists of many solutions that are optimal for very small regions of the weight space, such as solution 484, which is only optimal for 0.29% of the weights considered (Table 3). This indicates that if a solution that values yield highly is desired, then there are no robust solutions which are best for many weight combinations. However, since yield is likely the primary response, we may want to weigh it slightly more heavily than the other criteria, say around 50%–60% of the total weight with the remaining weight equally split between the other two criteria. Solution 79 is optimal for weightings $(w_1, w_2, w_3) = (0.5, 0.25, 0.25)$ and $(0.6, 0.2, 0.2)$, as well as similar weighting schemes.

The estimated responses for the solutions identified in Figure 6 are detailed in Table 3. Solution 484 has the highest estimated yield at the cost of both viscosity and molecular weight. Solutions 530–531 have estimated yields and molecular weights that are similar to those of solution 484 but have viscosities closer to 65. Solutions 90–92 are located in the lower left corner of the Pareto front in Figure 4. These solutions have the lowest estimated yields in Table 3 with the best molecular weight and good viscosity, in accordance with the weight combinations suggested in Figure 6. The remaining solutions (73–79) located on the bottom edge of the front in Figure 4 represent generally more balanced performance for all three responses.

Figure 7 displays the trade-off plot for the solutions that are optimal for at least one set of weights using the multiplicative DF. Those most robust solutions as identified by the mixture plot (those with at least 1% of the total simplex area) are represented by the larger, darker symbols, and solution 484 (of potential interest if yield is highly desired) is indicated with an open symbol. The innermost axes on Figure 7 represent the scaled values of the three criteria, with 1 corresponding to the best value of each criterion and 0 the worst. The remaining axes detail

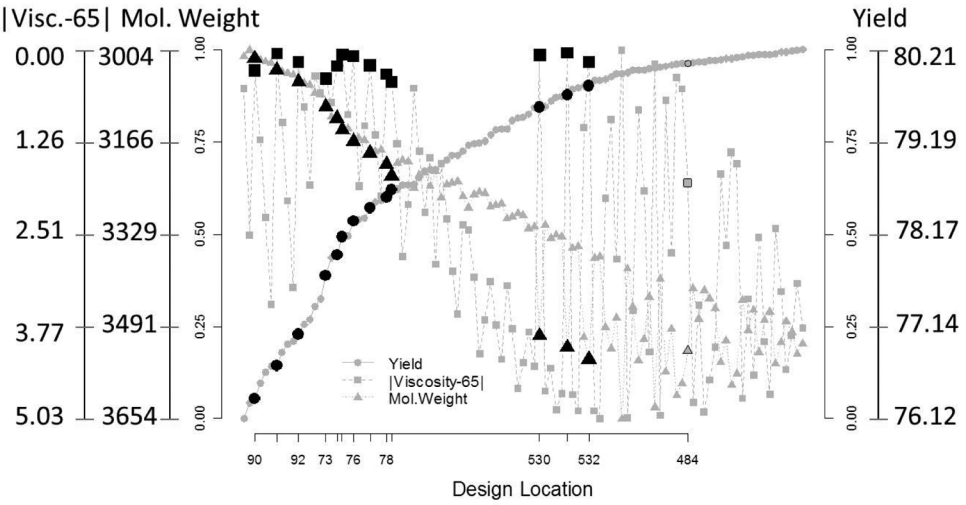

FIGURE 7 **Trade-off plot for the multiplicative form of DF (solutions numbered in Figure 6 are highlighted in black or open symbols).**

the ranges of the actual criteria values. The solutions are ordered, from left to right, based on the worst to best yield.

Solutions 90–92 perform poorly in terms of yield (very near the worst possible yield) but do well on the viscosity and molecular weight criteria (very near the best possible for each). Recall that these solutions were found to be optimal when the yield received minimal weight. With Solutions 73–79 (shown in sequential order in Figure 7 with solutions 73 and 78 labeled), viscosity has the best performance. The molecular weight performs reasonably well, and yield performs the worst of the three responses. Among these solutions, solution 76 has most balanced performance among the three responses. Solution 79 has better yield by sacrificing slightly on molecular weight and viscosity. Solutions 530–532 perform very well with respect to both yield and viscosity, in both cases achieving the best, or nearly the best, possible values while performing poorly for molecular weight. On the right side of Figure 7, there are a large number of solutions with good performance on yield and some oscillation in the viscosity and molecular weight responses, which leads to the many solutions optimal for small weight regions in Figure 6. Solution 484 is among these solutions, with near-optimal performance on the yield criterion, good performance on the viscosity criterion, and poor performance on molecular weight.

Synthesized efficiency plots (Lu and Anderson-Cook 2012) can be used to compare individual promising solutions to the best possible solution for different choices of weights. When using desirability functions to combine the three criteria into a single metric, the synthesized efficiency of solution j at the weight vector $\boldsymbol{w}$, relative to the optimal solution for weight $\boldsymbol{w}$, is defined as $SE(j,\boldsymbol{w}) = \frac{DF(j,\boldsymbol{w})}{max_j(DF(j,\boldsymbol{w}))}$. The synthesized efficiency plots for the five most promising solutions from Table 3, as well as solution 484, which emphasizes yield, are displayed in Figure 8. The white–gray–black shading represents high to low synthesized efficiency, with each of the 20 shades of gray corresponding to a 5% band of synthesized efficiencies. The synthesized efficiency plots for solutions 75 and 76 (adjacent grid points that together account for roughly 34% of the area [see Table 3] in the mixture plot in Figure 6) look quite similar, with both having large white regions that indicates there are a large number of weight combinations for which they are at least 95% efficient relative to the best possible solution. These solutions are at least 80% efficient for 87% and 90% of the weighting area, respectively. The minimum efficiencies achieved by solutions 75 and 76 are 49% and 54%, respectively (hence the absence of dark gray and black in the synthesized efficiency plot). Solution 79 also has a large white region, though it is located more towards the yield corner than for solutions 75 and 76, as is also seen in the weight combinations where solution 79 is best in Figure 6. Solution 79 is at least 80% efficient for 90% of the weight combinations considered. The minimum efficiency for solution 79 is about 62%. Solutions 91 and 531 are at least 80% efficient for

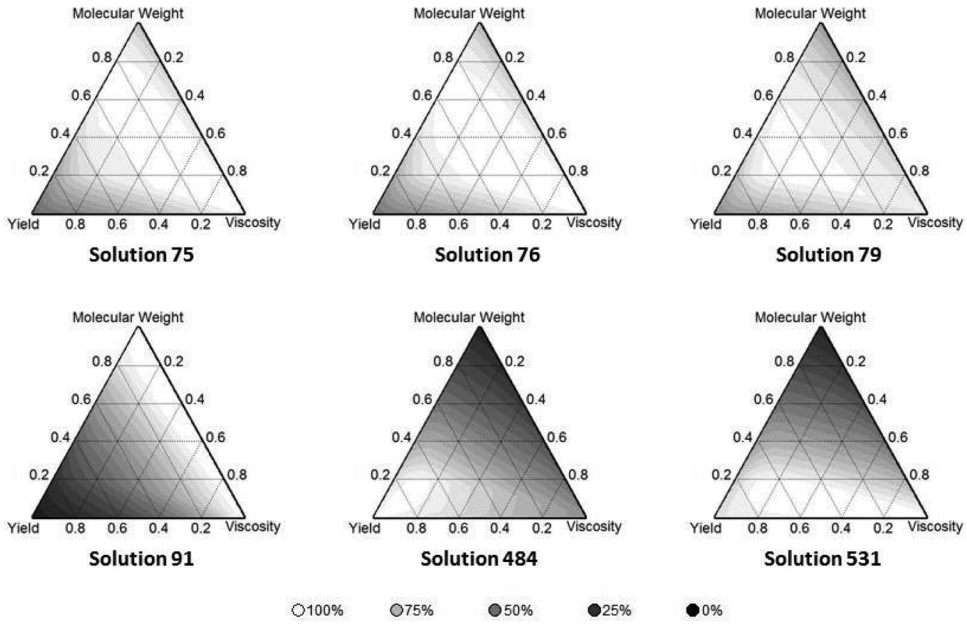

FIGURE 8 **Synthesized efficiency plots for some selected allocations.**

only 41% and 47% of the weight combinations, respectively, and the weight regions of best performance are in quite different locations compared the other highlighted solutions. Additionally, the synthesized efficiency plots for both solutions contain very large dark regions, indicating a large number of weight combinations for which the solutions perform very poorly compared to the best possible solution at that weight (as low as 15% efficiency in the yield corner for solution 91 and 19% in the molecular weight corner for solution 531). Solution 484 is at least 80% efficient for only 28% of the weight considered and has a minimum efficiency of 19% in the molecular weight vertex of Figure 8. If the process manager is interested in a specific region of the weighting area, the ideal solution can be selected based on its performance in that focused region.

To summarize the efficiencies across the weighting region, Lu et al. (2013) suggested the fraction of weighting space (FWS) plot, adapted from the fraction of design space plot (Zahran et al. 2003). It provides an overall, quantitative summary of the performance of an individual solution across the entire weighting space and can be used to easily compare competing solutions. The line for each solution plots the fraction of the weighting space for which the solution's synthesized efficiency is at least the specified percentage. For instance, examining the line for solution 91 in Figure 9 indicates that approximately 40% of weights have an efficiency higher than 80%, about 60% of weights have an efficiency higher than 65%, and about 80% of weights have an efficiency higher than approximately 45%. Further, the minimum efficiency can be observed at an FWS value of 1 (about 15% for solution 91).

Five of the selected solutions (all except solution 484) have very high synthesized efficiency for at least 20% of the weighting space. After that, the synthesized efficiency drops off relatively quickly for solutions 91 and 531, with solution 531 having slightly better synthesized efficiency for the remaining weighting space. Solutions 75 and 76 have similar synthesized efficiencies for the entire weighting space, with solution 76 having slightly better performance; the similarity of the curves for these solutions is reassuring as they are adjacent solutions on the grid in Figure 4. Solution 79 has slightly lower synthesized efficiency than both solutions 75 and 76 for up to about 80% of the weighting space, but after that point it has slightly higher synthesized efficiency and the best worst-case (minimum) efficiency of the solutions considered in Figure 9. Solution 484 has the lowest synthesized efficiency of the solutions considered for nearly the entire weighting space.

The figures discussed in this section provide a means of visualizing the Pareto front and examining the robustness and merits of different potential solutions. These figures, especially Figures 6–9, should be

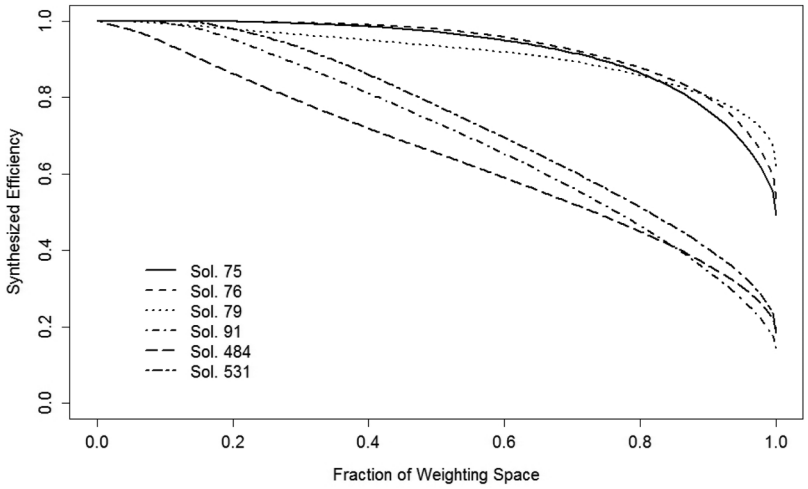

FIGURE 9 **Fraction of the weighting space (FWS) for which the synthesized efficiency exceeds a specified value for selected allocations.**

used to assist in the subjective decision-making process to find a good solution that matches user priorities. As an illustration, suppose that yield is the primary interest to the manager of this chemical process. Thus, the manager wants to choose as the optimal process setting a solution that performs well when the importance of yield is emphasized over the other two response variables, and perhaps the manager suggests relative weights on yield, viscosity, and molecular weight of around 0.6, 0.2, and 0.2, respectively. The mixture plot in Figure 6 suggests that solution 79 is the optimal solution around that region and, because of the size of the region, has some reasonable robustness to uncertainty in the manager-specified weight. Figure 7 shows the actual criterion values of the solution, relative to the ranges observed for other possible solutions on the Pareto front. Figures 8 and 9 suggest that solution 79 has good performance not only for the likely focused region of interest but also across the entire weighting space. Hence, by beginning with a region of interest in the weight space that matches the manager's priorities, solution 79 is found to be the dominating choice for the manager of this chemical process. We note that if the manager used the multiplicative desirability function approach with this weighting scheme, the same solution would be identified. However, the desirability function approach would not allow the manager to assess the robustness of the solution to uncertainty in the specified weight or to examine the trade-offs between the criteria and the performance of this solution relative to other solutions.

COMPARISON OF PARETO SOLUTIONS TO OTHER METHODS

In this section we compare the performance of the promising solutions identified in the previous subsection to those suggested in Myers et al. (2009). Figure 9 displays the synthesized efficiency of the four solutions in Table 2. Immediately obvious is the general dark coloring of three of the four solutions from Table 2 (both of those found via constrained optimization and the second desirability solution, the latter of which is not located on the front in Figure 4). The most promising of these solutions is the first desirability function solution (inverted triangular symbol in Figure 4). This solution lies in relatively close proximity to solution 79 on the grid and, not surprisingly, the synthesized efficiency plots for the two solutions look similar. The first desirability solution has at least 80% efficiency for about 88% of the weight combinations considered and has a minimum efficiency of 60%.

As noted in Figure 10, the FWS plot in Figure 11 suggests that the first desirability function solution from Table 2 performs comparably to solution 79, with solution 79 being slightly better for at least half of the weighting space. Interestingly, the other three solutions from Table 2 have considerably lower synthesized efficiency for much of the weighting space than the solutions highlighted from the Pareto set (with the exception of solution 484, which performs only slightly better than the constrained optimization solutions). However, these three solutions eventually surpass solutions 91, 484, and 531 and

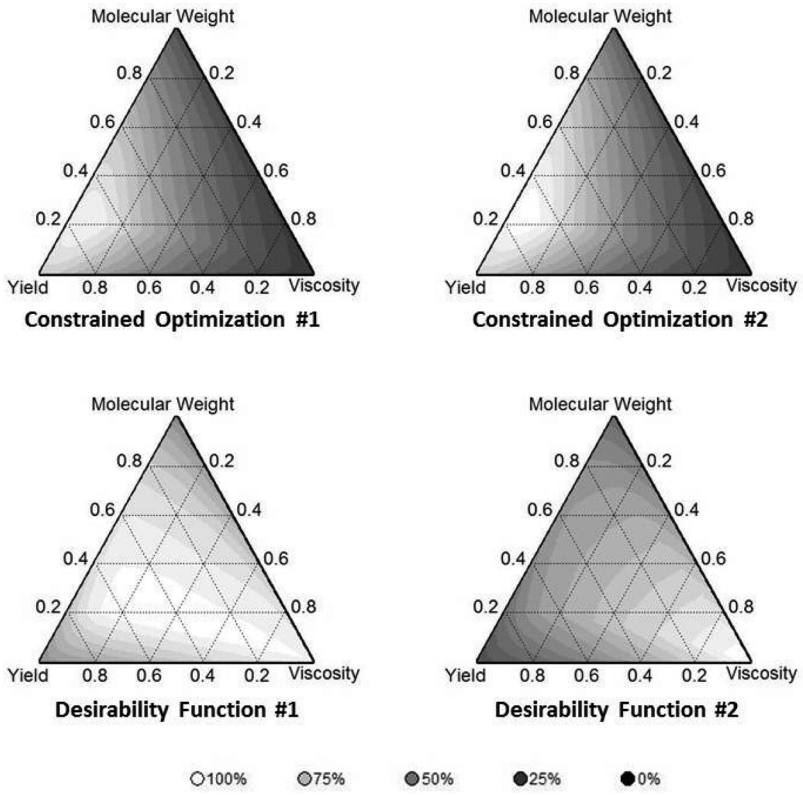

FIGURE 10 **Synthesized efficiency plots for the solutions presented in Table 2.**

actually have better worst-case (minimum) efficiency than any of these three solutions.

INVESTIGATING THE IMPACT OF PREDICTED RESPONSE VARIABILITY ON THE PARETO FRONT

In the section Pareto Front Multiple Objective Optimization, the Pareto front was identified based on the estimated responses at each point on the grid. However, when the goal of the study is to find a best condition for future operation in a process, there is no guarantee that future observed responses will be equal to these estimated responses when the process is run at a chosen design location due to the existence of natural variability in any process and the uncertainty associated with the estimated reponses. In this section we consider the impact that

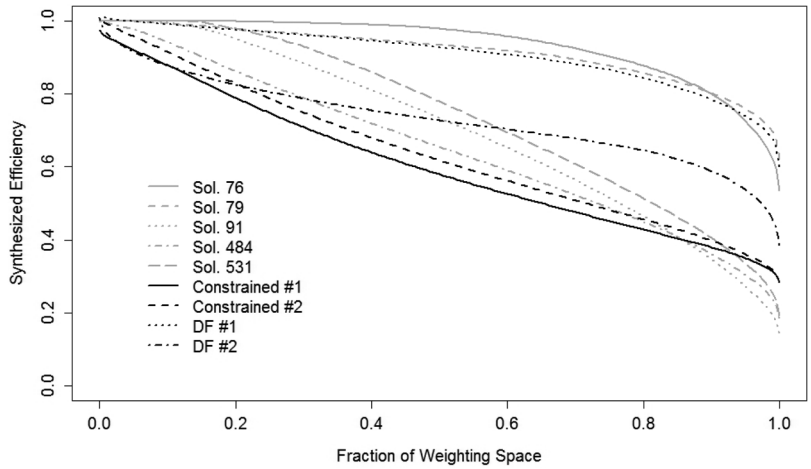

FIGURE 11 **FWS plot comparing selected solutions using the Pareto front approach (gray lines) to the solutions from Table 2 (black lines).**

variability in the prediction of future responses has on the Pareto front and the design location selected as optimal for the process.

Consider fitting a linear model of the form

$$\boldsymbol{Y} = \boldsymbol{X}\boldsymbol{\beta} + \epsilon,$$

where $\boldsymbol{Y}$ is an $n \times 1$ vector of the responses, $\boldsymbol{X}$ is the $n \times p$ model matrix, $\boldsymbol{\beta}$ is the $p \times 1$ parameter vector, and ϵ is an $n \times 1$ vector of independent and identically distributed random errors. Suppose it is of interest to predict the response, $\hat{Y}$, at a specific combination of the input variables $\boldsymbol{x}_0$, where $x_0' = (x_{01}, x_{02}, \ldots, x_{0p})$ is expected to match the model form. This prediction is given by $\hat{Y} = \boldsymbol{x_0'}\hat{\boldsymbol{\beta}}$, and a 95% two-sided prediction interval for the response at input vector x_0 is given by

$$\boldsymbol{x_0'}\hat{\boldsymbol{\beta}} \pm t_{0.975,n-p}\sqrt{MSE\left(1 + \boldsymbol{x_0'}(\boldsymbol{X'X})^{-1}\boldsymbol{x_0}\right)}.$$

In the context of our example, suppose we want to use the fitted model from the Introduction to predict the yield at $x_1 = 0.5$ and $x_2 = -1$ (a time of 87.5 min and temperature of 170°F). Thus, $\boldsymbol{x_0'} = (1, 0.5, -1, -0.5, 0.25, 1)$. The predicted yield at this setting is 78.45, and a 95% prediction interval for the yield at this setting is (77.73, 79.18), indicating that about 95% of yields observed at this setting are expected to be in this range. Note that the natural variability and estimation uncertainty of each of the responses is potentially different and so the prediction intervals will reflect this with different widths. In addition, the prediction variance of observations changes depending upon where we are in the design region—with best prediction at the center (0, 0) and worst prediction at the edges.

In the Pareto Front Multiple Objective Optimization section, the Pareto front was based on the mean estimated responses at each grid point. We might think of this as an estimate of the "typical" performance of each of the responses. Here we consider the impact of the variability in the predicted responses by using prediction intervals, such as the above, to select a conservative or worst-case estimate for the predicted response. In the case of yield, which is being maximized, we use the lower bound on the 95% prediction interval as our worst-case estimate of the response. Since we are minimizing molecular weight, we choose the upper bound of the prediction interval as a worst-case estimate of the molecular weight response. Finally, in the case of viscosity, where we are attempting to hit a target, we consider both bounds of the prediction interval and use the one that is furthest from the target viscosity of 65. These worst-case estimates, which balance the different precisions of estimation from the various responses as well as where we are in the design space, were then used to identify the solutions on the Pareto front (Figure 12).

In this application, the shape of the front did not change substantially when the worst-case predicted responses were used in place of the mean-estimated response. There were three points that were on the mean-estimated front but not on the worst-case response front (identified with open diamond symbols in Figure 12). Additionally, many of the same design locations from Figure 4 are flagged in Figure 12 as being optimal for a relatively large percentage of the different weighting combinations considered. The primary difference is that a new region, solutions 510 and 511, is identified; as indicated in Table 4, these solutions, which emphasize yield,

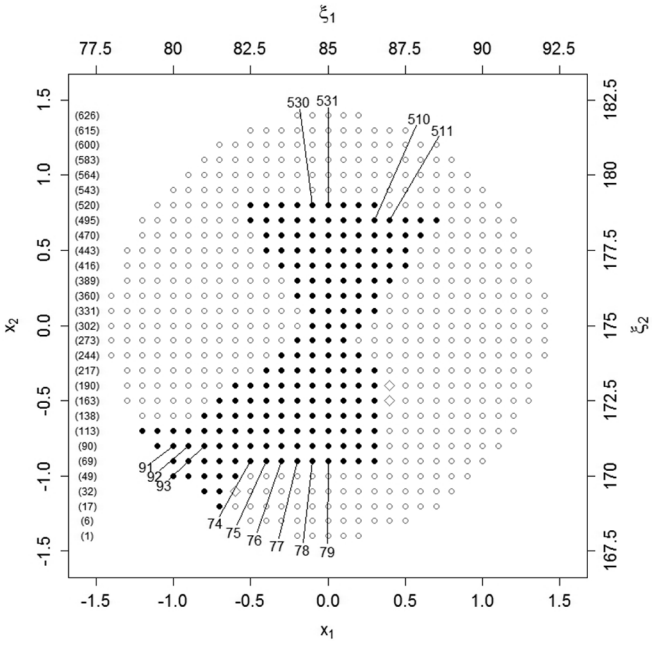

FIGURE 12 **Pareto front based on worst-case estimates of the predicted response. Labeled solutions are those identified as optimal for at least 1% of weights when the multiplicative form of the DF is used. Solutions on the mean-estimated response surface Pareto front but not on the worst-case front are identified with open diamond symbols.**

TABLE 4 The 13 Solutions Identified as Optimal for more than 1% of the Weights Considered in the Multiplicative Mixture Plot (Figure A1 in the Appendix) Based on Worst-Case Prediction Interval Bounds

Solution #	% Area in mixture (Figure A1)	Coded variables		Natural variables		Worst-case response estimates		
		x_1	x_2	ξ_1	ξ_2	$\hat{y}_1^C$	$\hat{y}_2^C$	$\hat{y}_3^C$
74	2.26	−0.5	−0.9	82.5	170.5	77.22	70.87	3,529.80
75	15.93	−0.4	−0.9	83	170.5	77.43	70.98	3,548.42
76	19.06	−0.3	−0.9	83.5	170.5	77.61	59.07	3,567.46
77	5.67	−0.2	−0.9	84	170.5	77.75	59.22	3,586.91
78	4.71	−0.1	−0.9	84.5	170.5	77.87	59.35	3,606.79
79	2.67	0	−0.9	85	170.5	77.97	59.46	3,627.09
91	3.52	−1	−0.8	80	171	75.95	71.45	3,456.97
92	3.51	−0.9	−0.8	80.5	171	76.31	58.81	3,473.59
93	1.14	−0.8	−0.8	81	171	76.64	59.14	3,490.59
510	1.08	0.3	0.7	86.5	178.5	79.35	59.78	3,967.49
511	1.13	0.4	0.7	87	178.5	79.36	59.61	3,989.51
530	1.79	−0.1	0.8	84.5	179	78.88	59.15	3,904.68
531	12.14	0	0.8	85	179	79.02	70.88	3,924.98

are optimal for 1.08% and 1.13% of the weights considered, respectively. The mixture and trade-off plots for the optimal solutions are displayed in Figures A1 and A2 in the Appendix.

It is helpful to quantify the potential impact from variability of the predicted responses on decision making. By comparing the worst-case predicted response estimates in Table 4 with the mean-estimated response in Table 3, we see dramatically different variability associated with the three responses. The worst-case estimates for yield for the solutions in Table 4 decreased by less than 1%. The worst-case viscosity estimates changed by 9%–11% from the mean estimates. The worst-case estimates for molecular weight increased by 11%–13% when compared to the mean case. We note that the dramatically different variabilities for the three responses are illustrated by the very different mean squared errors for the estimated models (the mean square errors for the yield, viscosity, and molecular weight models are 0.0709, 5.175, and 27431, respectively).

The approach to decision making taken in this article is to look at both the mean-estimated response and a measure of the worst-case estimated performance for the different responses. This provides information about the Pareto front choices across the range of uncertainty associated with the predicted values. In this example, the suggested input combinations that are best for both cases are quite similar, although the range of predicted values for each response varies considerably. However, the practitioner can feel quite confident that the locations identified are suitable for both typical and worst-case values of the responses. If the results had not been similar, the experimenter would then have needed to decide whether focusing on the typical results or protecting against worst-case outcomes is a higher priority when selecting an optimal combination of input levels.

In considering the impact of response variability and estimate uncertainty, it is important to examine several aspects of the optimization. In the objective phase of the process, the Pareto front solutions could change with different realized values of the estimated parameters. In the subjective phase, the designs that are best for a given weight combination of the criteria may also vary due to the change of the Pareto front. Additionally, once we have selected a particular "best" location, the range of response values is an important consideration. For our example, the yield response has relatively little associated variability, whereas the molecular weight experiences the most extensive possible fluctuations. The mean and worst-case approaches allow us to examine each of these aspects in a simple way, but there are certainly a variety of alternate approaches to looking at variability and its potential impact on decision making.

DISCUSSION AND CONCLUSIONS

The two-stage Pareto front optimization approach can facilitate improved decision making for multiple response optimization and provides an alternative to constrained optimization and desirability function approaches. In the first objective stage, inferior candidates are removed from consideration, allowing the focus to shift to the more promising alternatives. In the subjective stage, the promising candidates can be compared and the ranges and trade-offs of the criteria examined to help refine the priorities of the study. The graphical summaries highlight which input combinations perform well for the preferred weighting choices of the responses and how robust these combinations are across alternative prioritizations. The summaries help both with the decision-making process as well as provide supporting documentation to help persuade others about the merits of the decision.

One of the most important steps when using this approach is to specify the criteria over which the optimization should be performed. In our example, we focused on maximizing yield, getting close to the target viscosity of 65, and minimizing molecular weight. If, as was alternately suggested in Myers et al. (2009), we had changed the requirement for molecular weight to being in the range 3,200 to 3,400, with the ideal of 3,300, then the resulting Pareto front changes substantially. In Figure 13, we see that while some of the locations remain similar (those centered around $(x_1,\ x_2) = (0,\ 0.8)$), other new locations emerge as promising candidates (for instance, around $(x_1, x_2) = (-1, 0.7)$ and in the lower right corner of the design space). These Pareto front locations overlap well with the solutions identified in Myers et al. (2009) for this formulation of the problem. This should serve as a cautionary tale for practitioners to think carefully about what the objectives of the optimization are and then formulate the quantitative criteria to best match these goals.

Another important consideration is whether there are any constraints on how precisely the input factor levels can be set in the experiment. In such a case, the coarseness of the grid for approximating the response surfaces should match these constraints. Chapman et al. (2013) investigated using a coarser grid to estimate the response surfaces in this application. They found that the use of the coarser grid identified near-optimal solutions and missed

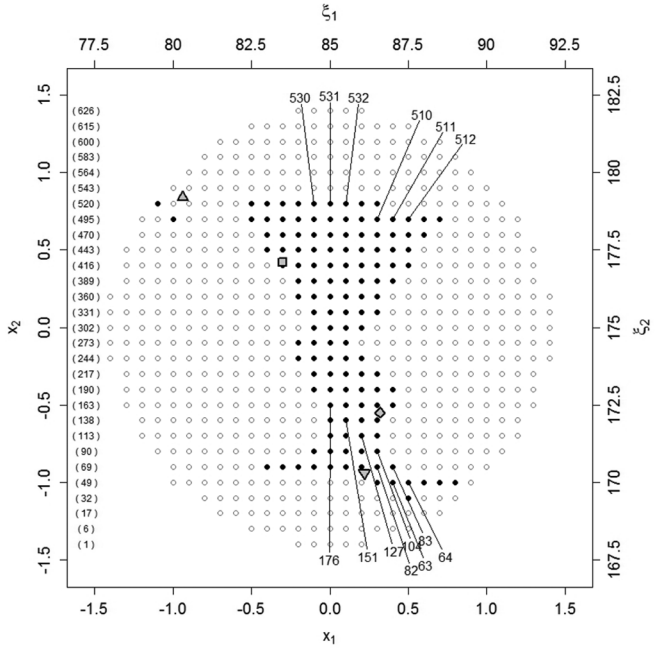

FIGURE 13 **Impact of slightly modifying the optimization problem on the Pareto front.**

the overall optimal choice. However, a coarse grid is computationally more efficient for identifying the larger region of the Pareto front and promising solutions. The experimenter then has the flexibility of fine-tuning the top performance choices for finding the best overall solution.

In this example, there are only two input factors over which to optimize the three responses. When considering the scalability of the problem, both the number of input factors as well as the number of criteria over which to optimize should be considered. First, we consider the number of inputs. When there are only two inputs, visualization of each of the response surfaces as well as the Pareto front locations in the design space is relatively simple. When the number of factors increases beyond two, some of the graphics need to be adapted. The contour plots of each individual response become problematic, and a dynamic summary, such as the profiler in JMP (version 9, SAS Institute, Cary, NC) can allow more flexible exploration. Of the Pareto approach plots, only the figures displaying the design locations, such as Figure 4, need to be changed. With three or more input factors, a summary table may provide the simplest summary of the location of the front. Alternately, dynamic rotating plots in many statistical software packages

would allow three of the dimensions to be viewed simultaneously.

Second, we consider changes in the number of criteria considered. Finding the Pareto front based on an increasing number of criteria remains straightforward, although the computational burden of fully populating the front will grow. Lu and Anderson-Cook (2013) showed how the mixture plot (Figure 6), trade-off plot (Figure 7), and synthesized efficiency plot (Figure 8) can be adapted to accommodate four criteria. The FWS plot of Figure 9 remains unchanged regardless of the number of criteria considered. A parallel plot (Lu and Anderson-Cook 2013) can be used to show the criteria values and their interrelationship and trade-offs for any number of criteria. If too many criteria are considered, the number of candidate solutions will increase substantially, making effective comparisons between alternatives difficult. Consequently, it is important to carefully bound the number of responses to consider, without losing the ability to solve the problem of interest.

The Pareto front optimization approach for multiple responses provides a strategy for identifying and comparing the performance of several preferred input combinations. The strategy of examining the front for both the mean-estimated responses as well as a worst-case percentile allows for the estimation uncertainty and variation in the responses to be taken into account, and the range of values to expect for the chosen solution is easily identified. If, as in this case, the fronts for both of these cases align, then the decision making for the practitioner is simple. However, we anticipate that there will be many situations when the fronts identified differ. In such situations, the practitioner should carefully consider whether primary interest lies in focusing on average or worst-case performance.

R code (R Development Core Team 2012) for implementing the methods discussed in this article is available upon request (jchapman@stlawu.edu).

ABOUT THE AUTHORS

Dr. Jessica L. Chapman is an assistant professor in the Department of Mathematics, Computer Science, and Statistics at St. Lawrence University in Canton, NY. She earned a doctorate in statistics from Iowa State University.

Dr. Lu Lu is a visiting assistant professor in the Department of Mathematics and Statistics at the University of South Florida. She earned a doctorate in statistics from Iowa State University.

Dr. Christine M. Anderson-Cook is a research scientist in the statistical sciences group at Los Alamos National Laboratory in Los Alamos, New Mexico. She earned a doctorate in statistics from the University of Waterloo in Ontario. She is a fellow of both ASQ and the American Statistical Association.

REFERENCES

Carlyle, M. W., Montgomery, D. C., Runger, G. C. (2000). Optimization problems and methods in quality control and improvement. *Journal of Quality Technology*, 32(1):1–17.

Chapman, J. L., Lu, L., Anderson-Cook, C. M. (2013). Process optimization for multiple responses utilizing the Pareto front approach. Los Alamos National Laboratory Technical Report LA-UR 13–22519.

Cornell, J. (2002). *Experiments with Mixtures: Design, Models, and the Analysis of Mixture Data*, 3rd ed. New York: Wiley.

Derringer, G., Suich, R. (1980). Simultaneous optimization of several response variables. *Journal of Quality Technology*, 12:214–219.

Gronwald, W., Hohm, T., Hoffmann, D. (2008). Evolutionary Pareto-optimization of stably folding peptides. *BMC-Bioinformatics*, 9:109.

Kasprzak, E. M., Lewis, K. E. (2001). Pareto analysis in multiple optimization using the collinearity theorem and scaling method. *Structural Multidisciplinary Optimization*, 22:208–218.

Lu, L., Anderson-Cook, C. M. (2012). Rethinking the optimal response surface design for a first-order model with two-factor interactions, when protecting against curvature. *Quality Engineering*, 24:404–422.

Lu, L., Anderson-Cook, C. M. (2013). Balancing multiple criteria incorporating cost using Pareto front optimization for split-plot designed experiments. *Quality and Reliability Engineering International*, 30(1):37–55.

Lu, L., Anderson-Cook, C. M., Robinson, T. J. (2011). Optimization of designed experiments based on multiple criteria utilizing a Pareto frontier. *Technometrics*, 53:353–365.

Lu, L., Chapman, J. L., Anderson-Cook, C. M. (2013). A case study on selecting a best allocation of new data for improving estimation precision of system and sub-system reliability using Pareto fronts. *Technometrics*, 55(4):473–487.

Myers, R. H., Montgomery, D. C., Anderson-Cook, C. M. (2009). *Response Surface Methodology*. Hoboken, NJ: Wiley.

R Development Core Team. (2012). *R: A Language and Environment for Statistical Computing*. Vienna, Austria: R Foundation for Statistical Computing. Available at: http://www.R-project.org/. Last accessed January 20, 2013.

Trautmann, H., Mehnen, J. (2009). Preference-based Pareto optimization in certain and noisy environments. *Engineering Optimization*, 41:23–38.

Zahran, A., Anderson-Cook, C. M., Myers, R. H. (2003). Fraction of design space to assess prediction capability of response surface designs. *Journal of Quality Technology*, 35:377–386.

APPENDIX

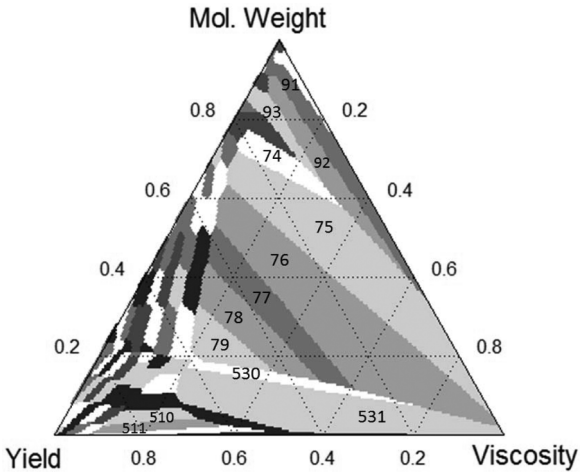

FIGURE A1 **Mixture plot for multiplicative desirability based on worst-case prediction of the response.**

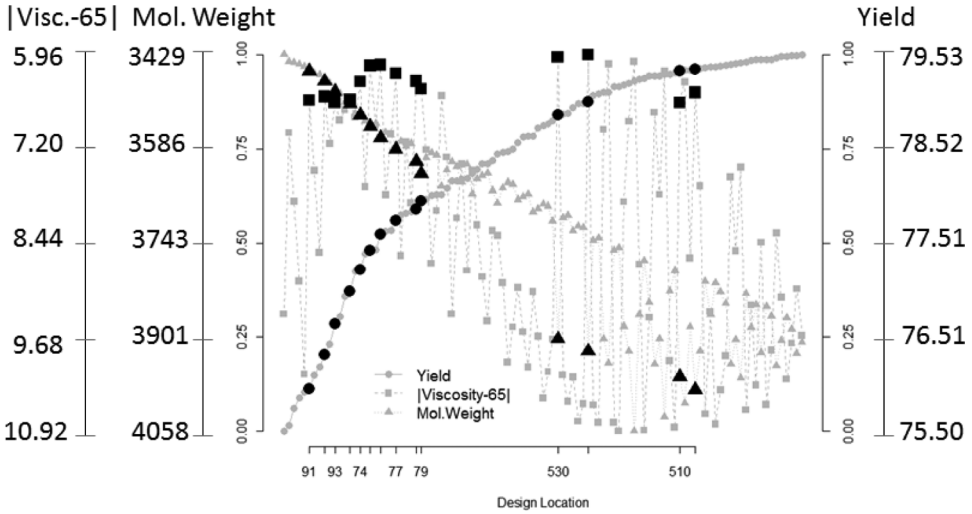

FIGURE A2 **Trade-off plot for multiplicative desirability when the worst-case prediction of the responses is considered.**